Phonon dispersion in red mercuric iodide

Hock-Kee Sim* and Yia-Chung Chang
Department of Physics and Materials Research Laboratory, University of Illinois at Urbana-Champaign, Urbana, Illinois 61801

R. B. James
Physical Sciences Department, Sandia National Laboratories, P. O. Box 969, Livermore, California 94550
(Received 28 June 1993)

We present theoretical studies of phonon modes of undoped HgI_2 in its red tetragonal form. A rigid-ion model including the Coulomb interaction is used which gives the best fit to the neutron scattering, infrared reflectivity, and Raman scattering data. The calculated sound velocities are also in accord with experiment.

I. INTRODUCTION

Red mercuric iodide (HgI_2) is a semiconductor which shows great potential for γ- and x-ray-spectrometry applications.[1-24] The electronic structures of the system have recently been studied by a relativistic linearized augmented-plane-wave method[25] and by an empirical pseudopotential method.[26] However, no theoretical studies on the phonon modes have been reported so far to our knowledge. Among the known experimental results on HgI_2 phonon spectra, only six low-lying branches have been measured by inelastic neutron scattering.[27] The measurements were along the two high-symmetry directions, i.e., Δ and Λ, in the reciprocal lattice space. Thus far, infrared[28] and Raman measurements[29,30] have only dealt with the higher-frequency modes at small wave vectors. In this paper, we present a theoretical study of the phonon dispersion curves by using a rigid-ion model similar to the one described in Ref. 31. We show that the model gives a good fit to the neutron scattering, infrared reflectivity, and Raman scattering data when the long-range Coulomb interaction and short-range force constants up to second-nearest-neighbor distances are included.

II. THEORETICAL MODEL

HgI_2 is a tetragonal crystal whose unit cell consists of two Hg and four I atoms as illustrated in Fig. 1, with lattice constants $a = b = 4.37$ Å, and $c = 12.44$ Å. The lattice has inversion symmetry about the midpoint between two neighboring Hg atoms. It is convenient to choose a tetragonal unit cell in which the four corners are occupied by Hg atoms. The x, y, and z axes are chosen to be parallel to the lattice vectors **a**, **b**, and **c**. If the origin is chosen at the center of the tetragon, the atomic positions of the two Hg atoms are (0,0,0) and $(\frac{a}{2},\frac{a}{2},\frac{c}{2})$ and those of the four I atoms are $(\frac{a}{2},0,-0.139c)$, $(\frac{a}{2},0,0.361c)$, $(0,\frac{a}{2},0.139c)$, and $(0,\frac{a}{2},-0.361c)$. The nearest-neighbor Hg-I, I-I, and Hg-Hg separations are 2.79 Å, 4.14 Å, and 4.37 Å, respectively. The next nearest-neighbor I-I and Hg-I separations are 4.37 Åand 4.99 Å, respectively. The third-nearest-neighbor I-I distance (4.64 Å) is less than the second-nearest-neighbor Hg-I distance. The third-neighbor force constants have not been included in the present calculation, since we find that the I-I interactions play a less significant role than the Hg-I interaction. There are two layers of I atoms between two closest Hg planes. As there are six atoms per unit cell, the total number of phonon branches is 18. The point group of the system is $\{E,\sigma_1,\sigma_2,S_1,S_2,S_3,\sigma_2S_1,S_1\sigma_2\}$, where E is the identity, σ_1 (σ_2) is a reflection about the y-z (x-z) plane, S_1 is a 90° rotation about the z axis followed by a reflection about the x-y plane, $S_2 = S_1^2$, and $S_3 = S_1^3$. The representation of the point group is given in Table I. In addition, the system has inversion symmetry as mentioned earlier. The complete group-theory analysis for the HgI_2 structure has been reported in Ref. 32.

With the use of symmetry, the dynamic matrices are readily obtained. The indices for atoms enclosed in the tetragonal unit cell are shown in Fig. 1. For equivalent atoms displaced by one lattice vector in the x-y plane

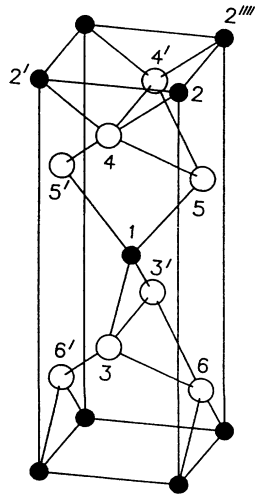

FIG. 1. Crystal structure of HgI_2.

TABLE I. The representation of the point group for HgI_2.

$$\sigma_1 = \begin{pmatrix} -1&0&0\\ 0&1&0\\ 0&0&1 \end{pmatrix}, \quad \sigma_2 = \begin{pmatrix} 1&0&0\\ 0&-1&0\\ 0&0&1 \end{pmatrix},$$

$$S_1 = \begin{pmatrix} 0&-1&0\\ 1&0&0\\ 0&0&-1 \end{pmatrix}, \quad S_2 = \begin{pmatrix} -1&0&0\\ 0&-1&0\\ 0&0&1 \end{pmatrix},$$

$$S_3 = \begin{pmatrix} 0&1&0\\ -1&0&0\\ 0&0&-1 \end{pmatrix}, \quad \sigma_2 S_1 = \begin{pmatrix} 0&-1&0\\ -1&0&0\\ 0&0&-1 \end{pmatrix},$$

$$S_1\sigma_2 = \begin{pmatrix} 0&1&0\\ 1&0&0\\ 0&0&-1 \end{pmatrix}, \quad E = \begin{pmatrix} 1&0&0\\ 0&1&0\\ 0&0&1 \end{pmatrix}.$$

($\pm\mathbf{a}$ or $\pm\mathbf{b}$), we denote them by the same index number with superscript $'$, $''$, $'''$, and $''''$ in a counterclockwise order when viewed from the top. For an equivalent atom displaced by a lattice vector $\mathbf{c}$, we denote it by the same index number with a bar on top.

For nearest-neighbor Hg-I interactions, we have

$$\Phi(1,5) = \begin{pmatrix} A_1&0&0\\ 0&B_1&D_1\\ 0&E_1&C_1 \end{pmatrix} = \sigma_2\Phi(1,5')\sigma_2^{-1}$$
$$= S_1\sigma_1\Phi(1,3)\sigma_1^{-1}S_1^{-1}$$
$$= S_1\Phi(1,3')S_1^{-1},$$

where we have used the fact that $\Phi(1,5)$ is invariant under σ_1 (see Fig. 1), which leads to vanishing xy, xz, yx, and zx components. With use of inversion, we further obtain

$$\Phi(2,4) = \Phi(1,5), \quad \Phi(2,4') = \Phi(1,5'),$$

$$\Phi(2,\bar{6}) = \Phi(1,3), \quad \Phi(2,\bar{6}'') = \Phi(1,3'),$$

where $\bar{6}$ denotes an atom equivalent to atom 6, but displaced by a lattice vector $\mathbf{c}$.

For nearest-neighbor I-I interactions, the use of inversion symmetry will lead to symmetric matrices, and we have

$$\Phi(3,6) = \begin{pmatrix} A_2&D_2&E_2\\ D_2&B_2&F_2\\ E_2&F_2&C_2 \end{pmatrix}$$
$$= \sigma_2\Phi(3,6')\sigma_2^{-1} = \sigma_1\Phi(3',6)\sigma_1^{-1} = \sigma_1\sigma_2\Phi(3',6')\sigma_2^{-1}\sigma_1^{-1} = S_1\Phi(5,4')S_1^{-1}$$
$$= \sigma_1 S_1\Phi(5,4)S_1^{-1}\sigma_1^{-1} = S_3\Phi(5',4)S_3^{-1} = \sigma_1 S_3\Phi(5',4')S_3^{-1}\sigma_1^{-1}.$$

For nearest-neighbor Hg-Hg interactions:

$$\Phi(1,1') = \begin{pmatrix} A_3&0&0\\ 0&B_3&D_3\\ 0&-D_3&C_3 \end{pmatrix}$$
$$= S_1\Phi(1,1'')S_1^{-1} = \sigma_2\Phi(1,1''')\sigma_2^{-1}$$
$$= S_1^{-1}\Phi(1,1'''')S_1,$$

where we have again used the fact that $\Phi(1,1')$ is invariant under σ_1. With use of inversion, we further obtain

$$\Phi(2,2') = \Phi(1,1'), \quad \Phi(2,2'') = \Phi(1,1''),$$

$$\Phi(2,2''') = \Phi(1,1'''), \quad \Phi(2,2'''') = \Phi(1,1'''').$$

For second-neighbor I-I interactions, we have

$$\Phi(3,3') = \begin{pmatrix} A_4&0&D_4\\ 0&B_4&0\\ -D_4&0&C_4 \end{pmatrix}$$
$$= S_1\Phi(5,5')S_1^{-1}$$
$$= \sigma_1\Phi(3,3''')\sigma_1^{-1}$$
$$= S_1\sigma_2\Phi(5,5''')\sigma_2{}^{-1}S_1{}^{-1},$$

$$\Phi(4,4') = \begin{pmatrix} A_5&0&D_5\\ 0&B_5&0\\ -D_5&0&C_5 \end{pmatrix}$$
$$= S_1\Phi(6,6')S_1^{-1}$$
$$= \sigma_1\Phi(4,4''')\sigma_1^{-1}$$
$$= S_1\sigma_2\Phi(6,6''')\sigma_2^{-1}S_1^{-1},$$

where we have used the fact that $\Phi(3,3')$ and $\Phi(4,4')$ are invariant under σ_2. With use of inversion, we further obtain

$$\Phi(4,4'''') = \Phi(5,5'), \quad \Phi(4,4'') = \Phi(5,5'''),$$

$$\Phi(6,6'') = \Phi(3,3'), \quad \Phi(6,6'''') = \Phi(3,3'''),$$

$$\Phi(5,5'') = \Phi(4,4'), \quad \Phi(5,5'''') = \Phi(4,4'''),$$

$$\Phi(3,3'''') = \Phi(6,6'), \quad \Phi(3,3'') = \Phi(6,6''').$$

For second-neighbor Hg-I interactions, we have

$$\Phi(1,6) = \begin{pmatrix} A_6&0&0\\ 0&B_6&D_6\\ 0&E_6&C_6 \end{pmatrix}$$
$$= \sigma_2\Phi(1,6')\sigma_2{}^{-1} = (S_1\sigma_1)\Phi(1,4)(S_1\sigma_1)^{-1}$$
$$= S_1\Phi(1,4')S_1^{-1},$$

and with use of inversion

$$\Phi(2,\bar{3}) = \Phi(1,6), \quad \Phi(2,\bar{3}'''') = \Phi(1,6'),$$

$$\Phi(2,5) = \Phi(1,4), \quad \Phi(2,5'') = \Phi(1,4').$$

The other interaction matrices not listed here can be obtained by using the Hermitian property of the dynamic matrix. Two constraints are imposed due to the translational invariance:

$$2(A_1 + B_1 + A_2 + B_2 + A_6 + B_6)$$

$$+A_3 + B_3 + A_4 + B_4 + A_5 + B_5 = 0,$$

$$2(C_1 + C_2 + C_6) + C_3 + C_4 + C_5 = 0.$$

In all, we have 26 independent adjustable parameters for describing the short-range interaction.

The long-range Coulomb interaction is calculated by the Ewald method, with $2e^*$ on Hg ions and $-e^*$ on I ions, where e^* is the effective charge transfer. We treat e^{*2}/ϵ as another adjustable parameter, where ϵ is the dielectric constant.

III. RESULTS AND DISCUSSION

The dispersion curves for the lowest ten phonon branches with six fitted to the neutron scattering data are shown in Fig. 2(a). The values of the parameters that provide the fitting are given in Table II. The branches are labeled by their symmetry representations according to the notation of Ref. 32 (i.e., $\Lambda_1, \Lambda_3, \Lambda_5$ along Γ-Z and $\Delta_1, \Delta_2, \Delta_3, \Delta_4$ along Γ-X). The Λ_5 is twofold, indicating transverse modes (with vibrations along x and y), where Λ_1 and Λ_3 are nondegenerate, indicating longitudinal modes (with vibrations along z). It is interesting to note that the two transverse modes do not coincide with each other at Z, while the two longitudinal modes do. This is a consequence of the symmetry of the crystal, since all irreducible representations are two dimensional for the space group at Z (see Ref. 32). The irreducible representations for the space group along the x axis are denoted Δ_1, Δ_2, Δ_3, and Δ_4 (all one dimensional). The Δ_2 and Δ_3 modes have symmetric and antisymmetric sums of y displacements, respectively. The Δ_1 mode contains an admixture of symmetric sums of x displacements (denoted the $x+$ component) and antisymmetric sums of z displacements (denoted the $z-$ component). Similarly, the Δ_4 mode contains an admixture of $x-$ and $z+$ components. An anticrossing behavior is found near $k_x = 0.15(2\pi/a)$ between an optical branch (with mostly the $z-$ component) and an acoustical branch (with mostly the $x+$ component), because they both have Δ_1 symmetry. All modes are doubly degenerate at X, since the irreducible representations for the space group at X are all two dimensional.

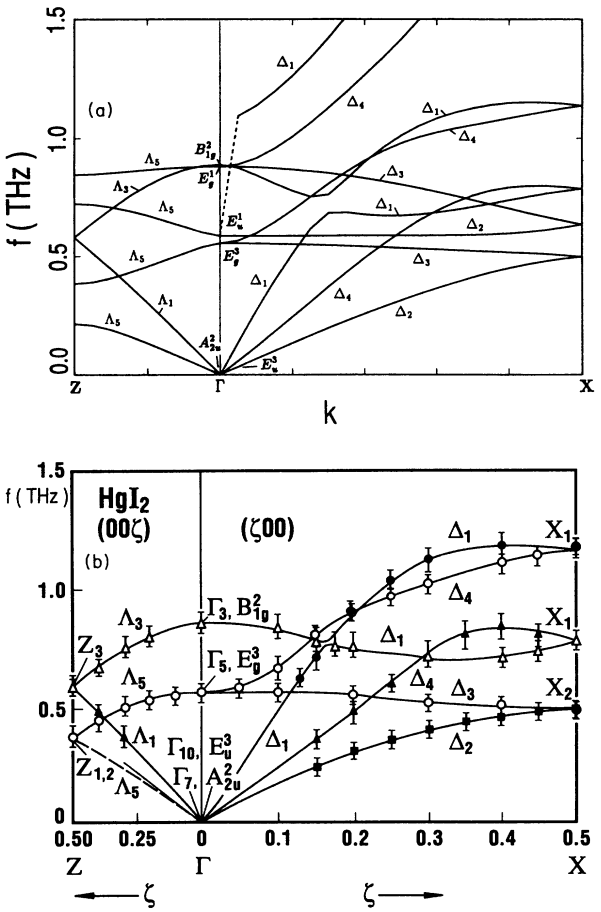

FIG. 2. Phonon dispersion curves for the lowest six branches (a) deduced from the present rigid-ion model and (b) taken from neutron scattering data of Ref. 27.

The symmetries of zone-center modes are labeled according to the notation used in Ref. 28. The E (E_g or E_u) modes are twofold degenerate when the wave vector approaches zero from the c axis, which corresponds to vibrations along the x and y directions. The A (A_{1g} or A_{2u}) and B (B_{1g} or B_{2u}) modes are nondegenerate, which corresponds to vibrations along the z axis. The subscribes g (gerade) and u (ungerade) denote even- and odd-parity modes with respect to the inversion center. Note that if we take symmetric and antisymmetric sums of displacements for atoms connected by the inversion

TABLE II. Parameters used in the rigid-ion model (measured in units of e^2/v_c, where v_c is the unit-cell volume).

A_1	B_1	C_1	D_1	E_1	
1.79347	-38.03613	-29.98524	17.45110	7.94596	
A_2	B_2	C_2	D_2	E_2	F_2
-8.86256	-0.23979	-4.91794	-77.76311	-6.85426	2.54791
A_3	D_3	A_4	B_4	C_4	D_4
7.01133	2.59967	-4.78037	-3.98045	-59.02348	-4.47929
A_5	B_5	C_5	D_5		
-27.74231	8.52126	19.87320	10.60398		
A_6	B_6	C_6	D_6	E_6	e^{*2}/ϵ
6.18102	-0.00736	2.48234	-18.88040	2.96253	0.26591

center, namely, those labeled by 1 and 2, 3 and 6, or 4 and 5 (see Fig. 1), the symmetric sums have odd parity (u modes) whereas the antisymmetric sums have even parity (g modes). A schematic diagram for atomic displacements in modes of various symmetries can be found in Fig. 1 of Ref. 28.

For comparison, the neutron scattering data[27,33] for six low-lying phonon branches are reproduced in Fig. 2(b). The six branches include three acoustical branches and three optical branches that are derived from the E_g^3 (the rigid-layer mode) and the B_{1g}^2 mode. The fit between theory and experiment for these modes is quite good. There are a few other branches derived from the E_u^1 mode and the E_g^1 mode, which lie among the above six branches. These modes have been obsevered by infrared or Raman measurements, but they are not observed by neutron scattering. We note that all these modes correspond to transverse vibrations (they have Λ_5 symmetry along z and Δ_2 or Δ_3 symmetries along x) when their frequencies fall within the range of observation reported in Ref. 27. It is conceivable that these transverse branches have too weak neutron scattering cross sections to be observed, since the one-phonon neutron scattering cross section is proportional to $|\mathbf{k}\cdot\epsilon_s(\mathbf{k})|^2$, where $\epsilon_s(\mathbf{k})$ is the phonon polarization vector.[34] The only branch (with Δ_1 symmetry) derived from the E_u^1 mode which has a longitudinal component lies far above the range of observation. Note that there is a distinct jump in frequency at the zone center for this branch which is indicated by a dashed line. This is due to the anisotropy effect to be discussed below. The sound velocities obtained here are listed in Table III and they are in good agreement with data.

The dispersion curves for all 18 branches are shown in Fig. 3. It is noted that the phonon frequencies for three particular branches are different when the wave vector approaches zero from different directions. Thus there are discontinuities in the dispersion curves at the Γ point. The dashed lines indicate where the discontinuities occur and how the branches are connected. This anisotropic behavior is typical for polar crystals with tetragonal symmetry[35] and for polar semiconductor superlattices.[36,37] The physical origin for this is explained in Refs. 36 and 37 in the context of the rigid-ion model. The anisotropy is caused by the long-range Coulomb interaction, which in the long-wavelength limit ($k \to 0$) takes the form[36]

$$C_{i,j}(\mathbf{k},l,l') = \frac{4\pi Q_l Q_{l'}}{v}\left(\frac{k_i k_j}{k^2} - \delta_{iz}\delta_{jz}\right) + D_{i,j}(l,l'),$$

where Q_l is the amount of charge transfer for ion l, v is the volume of the unit cell, and D is the Coulomb

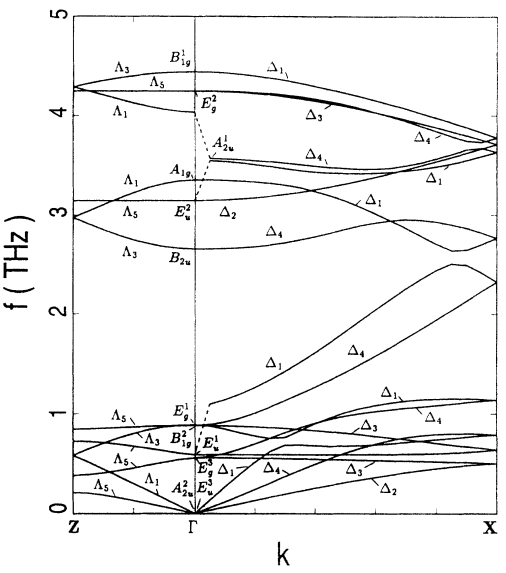

FIG. 3. Phonon dispersion curves for all 18 branches deduced from the present rigid-ion model.

part of the dynamic matrix of the crystal at $k = 0$ when approached from the (0,0,1) direction (c axis). The term $k_i k_j/k^2 \equiv S_{ij}$ takes the matrix form

$$\mathbf{S} = \begin{pmatrix} \sin^2\theta & 0 & \sin\theta\cos\theta \\ 0 & 0 & 0 \\ \sin\theta\cos\theta & 0 & \cos^2\theta - 1 \end{pmatrix}$$

for $\mathbf{k}$ in the x-z plane, where θ is the polar angle with respect to the z axis. This term gives rise to angular-dependent phonon frequencies at the zone center if the short-range part is not invariant under rotation. The angular dependence of phonon frequencies of HgI_2 is shown in Fig. 4. The three zero-frequency acoustic modes have no angular dependence, since in these modes all six ions vibrate in the same direction, which leads to zero polarization, defined as

$$\mathbf{P} = \sum_l \mathbf{u}_l Q_l,$$

where $\mathbf{u}_l$ is the displacement vector. Note that the angular-dependent part of the phonon frequency in a given mode is described by

$$\omega^2(\theta) = \text{const} \times \sum_{i,j} P_i^* S_{i,j}(\theta) P_j,$$

where P_i is the ith component of the polarization vector in the mode. The three branches (labeled E_u^1, E_u^2, and A_{2u}^1) that display significant angular disper-

TABLE III. Sound velocities (in 10^5 cm s^{-1}) of acoustic branches for HgI_2 obtained in the present rigid-ion model and from Ref. 27.

	$v_{l,\parallel}(001)$ (LA)	$v_{t,\perp}(001)$ (TA)	$v_{l,\perp}(100)$ [LA(x)]	$v_{t,\parallel}(001)$ [TA(z)]	$v_{t,\perp}(001)$ [TA(y)]
Expt.	1.55		2.23	1.07	0.74
Theory	1.51	0.67	2.34	1.01	0.58

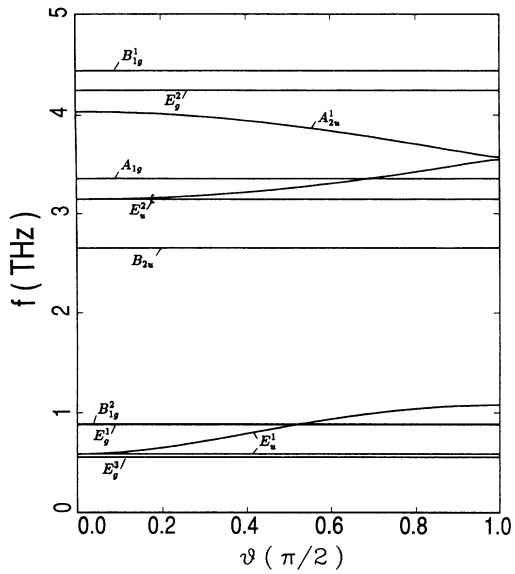

FIG. 4. Angular dispersion of phonon frequencies for HgI_2 deduced from the present rigid-ion model.

sion are modes with large strengths of polarization. In these modes, ions of opposite charges vibrate against each other. Thus they are also infrared active. The phonon frequencies of these infrared-active modes were observed[28] to be at 0.52, 3.14, and 3.76 THz. Our calculated frequencies for these three modes are 0.587, 3.145, and 3.57 THz, respectively, in fair agreement with experiment. Note that the A_{2u}^1 mode has a polarization vector parallel to the z axis. Thus the infrared measurement must be performed with incident radiation propagating perpendicular to the c axis, and we have used the calculated A_{2u}^1 frequency at $\theta = \pi/2$ to compare with experiment. To compare with experimental data for infrared- and Raman-active modes, we list the calculated phonon frequencies at the zone center in Table IV, in conjunction with experimental values. The agreement between theory and experiment is fairly good.

TABLE IV. Zone-center phonon frequencies (in THz) for HgI_2 obtained in the present rigid-ion model and from various experimental measurements. All but the A_{2u}^1 mode are calculated at $\theta = 0$. The A_{2u}^1 mode is calculated at $\theta = \pi/2$.

	E_u^1	E_g^3	B_{1g}^2	E_g^1	B_{2u}
Theory	0.587	0.556	0.889	0.881	2.653
Expt.	0.52[a]	0.56[b]	0.85[b]	0.87[c]	
	E_u^2	A_{1g}	A_{2u}^1	E_g^2	B_{1g}^1
Theory	3.145	3.352	3.570	4.245	4.437
Expt.	3.14[a]	3.42[c]	3.69[a]		4.38[d]

[a]Infrared reflectivity (Ref. 28).
[b]Neutron scattering (Ref. 27).
[c]Raman scattering (Ref. 29).
[d]Raman scattering (Ref. 27).

IV. CONCLUSIONS

We have calculated the phonon dispersion curves for HgI_2 by using a rigid-ion model, including the long-range Coulomb interaction. With 27 adjustable parameters, the fit of six low-lying branches to the neutron scattering data is very good. We found that as a result of crystal symmetry TA and TO modes do not coincide at Z whereas the LA and LO modes do. The angular dispersion of the phonon modes is studied, and three infrared-active modes are found which display large angular dispersion. The frequencies of these modes and all Raman-active modes are also in good agreement with experiment.

ACKNOWLEDGMENTS

This work was supported in part by the Department of Energy. The use of computing facilities of the University of Illinois Material Research Laboratory is acknowledged.

*Permanent address: Department of Physics, National University of Singapore, Singapore 0511.
[1]W. R. Willing, Nucl. Instrum. Methods **96**, 615 (1971).
[2]J. P. Ponpon, R. Stuck, P. Siffert, B. Meyer, and C. Schwab, IEEE Trans. Nucl. Sci. NS-**22**, 182 (1975).
[3]A. J. Dabrowski, W. M. Szymczyk, J. S. Iwanczyk, J. H. Kusmiss, W. Drummond, and L. Ames, Nucl. Instrum. Methods **213**, 89 (1983).
[4]S. P. Swierkowski, G. A. Armantrout, and R. Wichne, IEEE Trans. Nucl. Sci. NS-**21**, 302 (1974).
[5]J. H. Howes and J. Watling, in *Nuclear Radiation Detector Materials*, edited by E. E. Haller, H. W. Kraner, and W. A. Higinbotham, MRS Symposia Proceedings No. 16 (Materials Research Society, Pittsburgh, 1983), p. 207.
[6]H. L. Malm, T. W. Raudoff, M. Martina, and K. R. Zanio, IEEE Trans. Nucl. Sci. NS-**20**, 500 (1973).
[7]R. C. Whited and M. Schieber, Nucl. Instrum. Methods **162**, 119 (1979).
[8]B. V. Novikov and M. M. Pimonenko, Fiz. Tekh. Poluprovodn. **4**, 2077 (1970) [Sov. Phys. Semicond. **4**, 1785 (1971)].
[9]K. Kanzaki and I. Imai, J. Phys. Soc. Jpn. **32**, 1003 (1972).
[10]A. Anedda, F. Raga, E. Grilli, and M. Guzzi, Nuovo Cimento **38**, 439 (1977).
[11]P. D. Bloch, J. W. Hodby, C. Schwab, and D. W. Stacey, J. Phys. C **11**, 2579 (1978).
[12]C. Dlasi, S. Galassini, C. Manfredotti, G. Micocci, L. Ruggiero, and A. Tepore, Nucl. Instrum. Methods **150**, 103 (1978).
[13]U. Gelbert, Y. Yacoby, I. Beinglass, and A. Holzer, IEEE Trans. Nucl. Sci. NS-**24**, 135 (1977).
[14]J. C. Muller, A. Friant, and P. Siffert, Nucl. Instrum. Methods **150**, 97 (1978).
[15]M. Schieber, I. Beinglass, G. Dishon, A. Holzer, and G.

Yaron, Nucl. Instrum. Methods **150**, 71 (1978).
[16]A. Anedda, E. Grilli, M. Guzzi, F. Raga, and A. Serpi, Solid State Commun. **39**, 1121 (1981).
[17]T. Goto and A. Kasuya, J. Phys. Soc. Jpn. **50**, 520 (1981).
[18]S. R. Kurtz, R. C. Huges, C. Ortale, and W. F. Schnepple, J. Appl. Phys. **62**, 4308 (1987).
[19]D. Wong, X. J. Bao, T. E. Schlesinger, R. B. James, A. Cheng, C. Ortale, and L. van den Berg, Appl. Phys. Lett. **53**, 1536 (1988).
[20]R. B. James, X. J. Bao, T. E. Schlesinger, J. M. Markakis, A. Y. Cheng, and C. Ortale, J. Appl. Phys. **66**, 2578 (1989).
[21]R. B. James, X. J. Bao, T. E. Schlesinger, C. Ortale, and L. van den Berg, J. Appl. Phys. **67**, 2571 (1990).
[22]X. J. Bao, T. E. Schlesinger, R. B. James, R. H. Stulen, C. Ortale, and L. van den Berg, J. Appl. Phys. **68**, 86 (1990).
[23]L. R. Williams, R. J. M. Anderson, and M. J. Banet, Chem. Phys. Lett. **182**, 422 (1991).
[24]X. J. Bao, T. E. Schlesinger, R. B. James, G. L. Gentry, A. Y. Cheng, and C. Ortale, J. Appl. Phys. **69**, 4247 (1991).
[25]D. E. Turner and B. N. Harmon, Phys. Rev. B **40**, 10 516 (1989).
[26]Y. C. Chang and R. B. James, Phys. Rev. B **46**, 15 040 (1992).
[27]B. Prevot, C. Schwab, and B. Dorner, Phys. Status Solidi B **88**, 327 (1978).
[28]J. Biellmann and B. Prevot, Infrared Phys. **20**, 99 (1979).
[29]S. Nakashima and M. Balkanski, Phys. Rev. B **34**, 5801 (1986).
[30]N. Kuroda, T. Iwabuchi, and Y. Nishina, J. Phys. Soc. Jpn. **52**, 2419 (1983).
[31]K. Kunc, Ann. Phys. (Paris) **8**, 319 (1973).
[32]M. Sieskind, J. Phys. Chem. Solids **39**, 1251 (1978).
[33]*Landolt-Börnstein Numerical Data and Functional Relationships in Science and Technology*, edited by O. Madelung, Vol. 17 (Springer-Verlag, New York, 1984), p. 530.
[34]See, for example, N. W. Ashcroft and N. D. Mermin, *Solid State Physics* (Saunders, Philadelphia, 1976), p. 794.
[35]C. A. Arguelloo, D. L. Rousseau, and S. P. Porto, Phys. Rev. **181**, 1351 (1969).
[36]S. F. Ren, H. Chu, and Y. C. Chang, Phys. Rev. B **37**, 8899 (1988).
[37]H. Chu, S. F. Ren, and Y. C. Chang, Phys. Rev. B **37**, 10 746 (1988).